Click Here for Full Article

Predictions of the electrical conductivity and charging of the aerosols in Titan's nighttime atmosphere

R. C. Whitten,[1] W. J. Borucki,[2] and S. Tripathi[3]

[1]   The electrical conductivity and electrical charge on Titan's atmosphere are computed for altitudes between 0 and 400 km on the nightside for which the main source of ionization is galactic cosmic rays (GCR). Unlike the dayside, electrical charging of the aerosol particles at night is not only negative but also time-dependent. Hence a time-dependent model must be employed for computations of electron and ion densities as well as aerosol charging over the night hemisphere. After developing a method for computing the time-dependent charge states of the aerosol particles, we found that that at altitudes above about 60 km (the effusion range) the charging of the aerosols at the antisolar point is quite close to that at steady state; however, at lower altitudes where (the slow) diffusion of the electrons and ions prevails, the electron density is larger (and the charging of the aerosol particles is smaller) than at steady state. Because polycyclic aromatic hydrocarbons (PAHs) are expected in Titan's atmosphere and have been observed in the laboratory and found to be electrophillic, we have included the formation of negative ions in the aerosol charging model. Such ions are of major importance at night between about 170 and 360 km where they capture most of the negative charge. As a result they greatly reduce the electron density and thus the electrical conductivity in that altitude range. The charge distributions at 50 km (diffusion range), 150 km (effusion range with few negative ions), and 250 km (effusion range) are presented.

1.   Introduction

[2]   In a previous paper [*Borucki et al.*, 2006] we presented computational results for the charging of aerosols on the dayside of Titan and the formation of negative ions. We found that solar ultraviolet radiation at the distance of Titan from the Sun is sufficiently intense to produce a high-density ionosphere. Moreover, the ionization and ion loss processes occur so rapidly that assumption of steady state conditions is fully justified. Such high electron densities result from photoemission of electrons from aerosol particles in the Titan haze. On the nightside, however, the absence of solar radiation leads to much smaller electron densities since the only sources of ionization are galactic cosmic rays (GCR) and at altitudes above 350 km, precipitating electrons from Saturn's magnetosphere. Furthermore, steady state is no longer justified. The smaller electron densities lead to smaller charging of the aerosol particles and time dependence must be included in the computations. Moreover, negative ions formed by attachment of electrons to very small (embryo) particles are the dominant negative ions at some altitudes of 170 to 350 km. In addition, if the

work function of the aerosol particles exceeds the absorption energy cut-off for methane ($\sim$8.7 eV), a significant minor constituent, then steady state computations without solar radiation will apply to both the dayside and nightside of Titan. This paper presents computational results for both the antisolar meridian of Titan and for steady state conditions. We note that while we have not investigated the influence of particle charge on coagulation, it is likely to be important [see *Toon et al.*, 1992; *Cabane et al.*, 1992, 1993]. Whether the charge is positive or negative, it inhibits (or under some conditions may aid) the coagulation process. In turn the coagulation rate influences the size and abundance distributions, and the atmospheric temperature and circulation. These affects are important topics for future research.

## 2.   Atmospheric Environment and GCR Ionization

[3]   To calculate the conductivity of the atmosphere it is necessary to choose a standard atmosphere. Table A1 in Appendix A presents values of the temperature, pressure, and number density as a function of altitude taken from a recommended model atmosphere described by *Yelle et al.* [1996] and used in our previous paper [*Borucki et al.*, 2006] in which the origins of the model are explained.

[4]   The ionization rates due to bombardment of the atmosphere by galactic cosmic rays (GCR) were taken from those published earlier by *Borucki et al.* [1987] and are

[1]SETI Institute, Mountain View, California, USA.
[2]NASA Ames Research Center, Moffett Field, California, USA.
[3]Indian Institute of Technology, Kanpur, India.
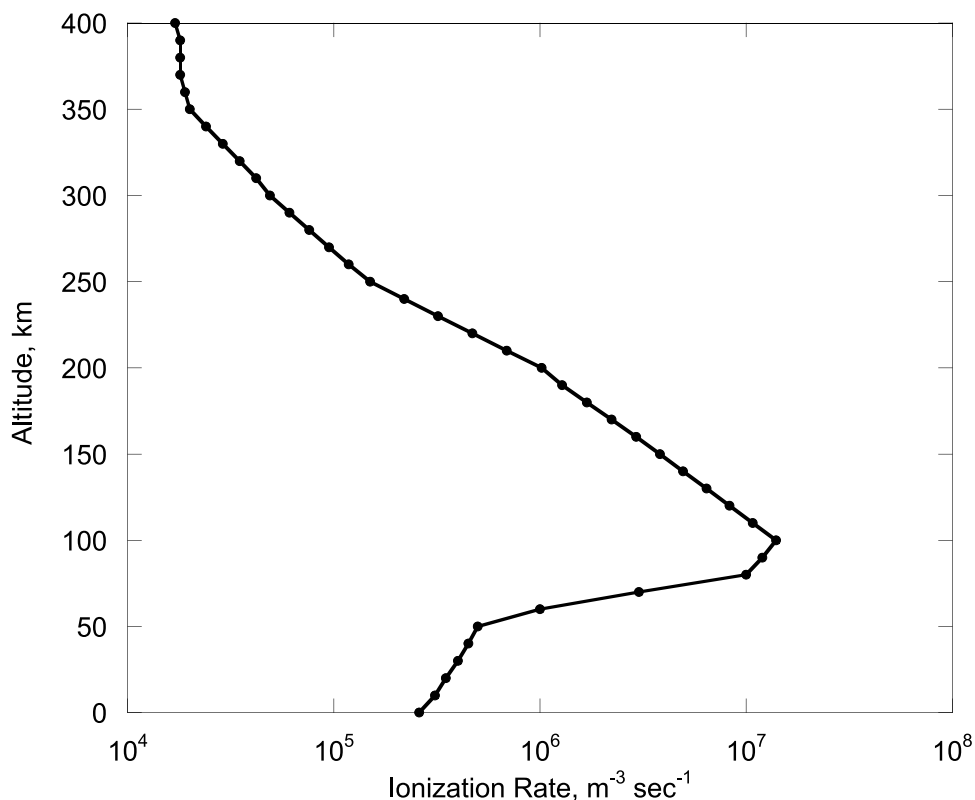
Figure 1. Ionization rate from galactic cosmic rays and from precipitating electrons as a function of altitude.

similar to those of *Molina-Cuberos et al.* [2000]. The ionization model for GCR is an adaptation of a model developed for Earth by *O'Brien* [1971, 1972, 1975a, 1975b].The contribution to ionization from precipitating particles from the Saturnian magnetosphere [*Krimingis et al.*, 1983; *Vogt et al.*, 1981] was included as described by *Borucki et al.* [1987]. Figure 1 shows the computed ionization rate versus altitude caused by energetic particles.

3. Aerosol Abundance

[5] In an earlier paper [*Borucki et al.*, 2006] we discussed the distribution of aerosols in the Titan atmosphere which is supported by spacecraft observations. Size information was derived from the data obtained from the Voyager photopolarimeter observations [*West et al.*, 1983]. Voyager high-phase-angle images [*Rages et al.*, 1983] and photometry and polarimetry measurements from Pioneer 11 [*Tomasko and Smith*, 1982]. Analysis of Voyager 2 images by *Rages and Pollack* [1983] indicate that between 220 km and 350 km the aerosol particles have radii near 0.3 microns and have number densities that range from about 2×10^5 particles m^{-3} at 350 km to 2×10^6 particles m^{-3} near 220 km. Because spacecraft measurements have not adequately determined the aerosol size distributions, shapes, abundances, or their variation with altitude above 120 km, the results of the theoretical model by *Toon et al.* [1992] are used to estimate these quantities.

[6] This model simulates the physics of production, growth and transport of the aerosol particles and is consistent with the spacecraft measurements. The particle size and number density data obtained from *Barth and Toon* [2003] were contained in 31 size bins. To facilitate the electrical charging computations the largest 31 bins were sorted into five size bins using the method discussed in section 5.2 of *Borucki et al.* [2006]. The approximate particle radii for each bin are presented in Table 1. We also include the estimated radius of the very small polycyclic aromatic hydrocarbon (PAH) particles. PAHs are expected in Titan's atmosphere. They have been observed in the laboratory and found to be electrophillic. Thus because they are small enough to be mobile, yet large enough to have many degrees of freedom for dissipation of the energy of attachment, we include them as negative ions. The PAHs are the smallest particle in the aerosol model developed by *Barth and Toon* [2003].

[7] Figure 2 shows the model aerosol size distributions as a function of altitude for several size bins. As expected, the smaller sizes are prevalent at the higher altitudes while the larger sizes are found mainly at lower altitudes. Maxima in abundances for the three largest size bins occur in the 50 to 120 km altitude range; i.e., at altitudes that the Huygens Atmosphere Structure Instrument (HASI) sampled. The very small polycyclic aromatic hydrocarbons (PAHs) are also

Table 1. Bin Number Versus Mean Particle Size

Bin Number	Approximate Mean Particle Diameter, microns
5	0.2
4	0.1
3	0.05
2	0.025
1	0.013
PAH	3×10^{-4}
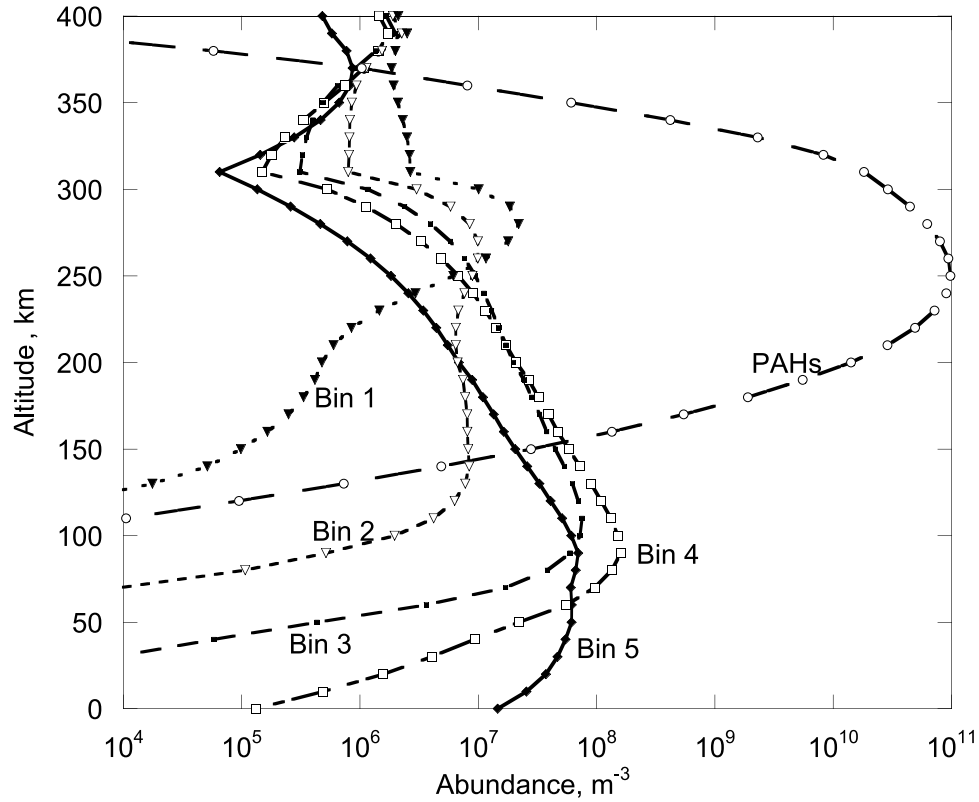
Figure 2. Aerosol and polycyclic aromatic hydrocarbons (PAH) Abundance.

plotted. As explained earlier, these particles can attach electrons and act like negative ions. The altitude distribution, which was also employed in *Borucki et al.* [2006], is subject to considerable uncertainty.

4. Time-Dependent Equations

[8] The nighttime time-dependent equations to be solved for the positive ion density, n_+, negative ion density, n_-, and total charge on the aerosol particles, z_a, are

$$\frac{dn_+}{dt} = q - \alpha_{+ION}n_e n_+ - \alpha_{-ION}n_- n_+ - d_{ion}n_+ \qquad (1)$$

$$\frac{dn_-}{dt} = \kappa n_{PAH}n_e - \alpha_{-ION}n_+ n_- - d_{negion}n_- \qquad (2)$$

$$z_a = \sum_k N_k^a \sum_l lP_{l,k} \qquad (3)$$

[9] The electron density, n_e, is computed by requiring local charge neutrality so that

$$n_e = z_a + n_+ - n_- \qquad (4)$$

[10] The electron density can also be computed from the equation

$$\frac{dn_e}{dt} = q - \alpha_{+ION}n_+ n_e - d_{ele}n_e - \kappa n_{PAH}n_e \qquad (5)$$

which we use to estimate the error in computed n_e.

[11] The other symbols in equations (1) through (4) have the following definitions:

q is the ionization rate due to galactic cosmic rays;

α_{+ION} is the electron-positive ion recombination coefficient;

α_{-ION} is the positive ion–negative ion recombination coefficient;

κ is the attachment coefficient for electrons to PAHs;

N_k^a is the aerosol particle density for radii of index k;

n_{pah} is the polycyclic aromatic hydrocarbon (PAH) particle density;

d_{ion} is the attachment rate (s^{-1}) for capture of positive ions by aerosol particles

$$d_{ion} = \sum_k N_k^a \sum_l P_{l,k}\nu_{l,k}^+ \qquad (6)$$

d_{ele} is the attachment rate (s^{-1}) of electrons by aerosol particles

$$d_{ele} = \sum_k N_k^a \sum_l P_{l,k}\nu_{l,k}^e \qquad (7)$$

d_{negion} is the attachment rate (s^{-1}) of negative ions by aerosol particles

$$d_{negion} = \sum_k N_k^a \sum_l P_{l,k}\nu_{l,k}^- \qquad (8)$$

$\nu_{l,k}^e$ is the electron capture rate for an aerosol particle with charge l and radius specified by k;

$\nu_{l,k}^+$ is the positive ion capture rate for an aerosol particle with charge l and radius specified by k;

$\nu_{l,k}^-$ is the negative ion capture rate for an aerosol particle with charge l and radius specified by k; and

$P_{l,k}$ is the probability of finding an aerosol particle of radius index k in charge state l.

[12] The foregoing equations are similar to those discussed by *Borucki et al.* [2006] except that photo emission required for daytime conditions is omitted. Although night fall occurs gradually, the positive charge due to photoelectric emission quickly decays after solar illumination is cut off. Thus we use a zero charge on all aerosols as an initial condition at the dusk terminator.

[13] The charge state of aerosol particles are functions of particle size and time. The time dependence occurs because the times required to reach charge equilibrium are of the same order of magnitude as the period of rotation. At altitudes below 60 km, relaxation times are even longer. Hence the calculation of a particle being in a particular charge state requires an appropriate algorithm to approximate time dependence. *Parthasarathy* [1976] derived a steady state recurrence relation to compute the build-up of electric charge on aerosol particles due to collision with electrons, negative ions, and positive ions.

$$P_{l,k}\left[\nu^e_{l,k}n_e + \nu^+_{l,k}n_+ + \nu^-_{l,k}n_-\right] = P_{l+1,k}\nu^e_{l+1,k}n_e + P_{l+1,k}\nu^-_{l+1,k}n_- + P_{l-1,k}\nu^+_{l-1,k}n_+ \quad (9)$$

where l is the number of electron charges and k is the particle size index. This recurrence expression can be rearranged (with l replaced by l−1 and negative ions included) to yield

$$P_{l,k} = \left[P_{l-1,k}\left(\nu^e_{l-1,k}n_e + \nu^+_{l-1,k}n_+ + \nu^-_{l-1,k}n_-\right) - P_{l-2,k}\nu^+_{l-2,k}n_+\right]/\left(\nu^e_{l,k}n_e + \nu^-_{l,k}n_-\right). \quad (10)$$

[14] Solutions to equation (10) are obtained by setting the $P_{l,k}$ for the lowest charge, e.g., $l = -15$, to zero, and $P_{l,k}$ for $l = -14$ to some very small positive value; then the recurrence relation is invoked to compute $P_{l,k}$ for the entire charge range. The two lowest charge values are adjusted until $P_{l,k}$ for the next higher l value is also very small. As with all probability distributions, the $P_{l,k}$ must be appropriately normalized such that

$$\sum_l P_{l,k} = 1 \quad (11)$$

[15] Because of the change in charge with time, Parthasarathy's relation equation (9) must be modified to reflect time dependence of the charge probability $P_{l,k}$ which can be expressed by the equation

$$\frac{dP_{l,k}}{dt} = P_{l+1,k}\left(\nu^e_{l+1,k}n_e + \nu^-_{l+1,k}n_-\right) + P_{l-1,k}\nu^+_{l-1,k}n_+ - P_{l,k}\left(\nu^e_{l,k}n_e + \nu^-_{l,k}n_- + \nu^+_{l,k}n_+\right) \quad (12)$$

[16] The discretization of equation (12) yields

$$\frac{dP_{l,k}}{dt} \rightarrow \left[P^i_{l,k} - P^{i-1}_{l,k}\right]/\Delta t \quad (13)$$

in which i represents the time step starting with 1. We found that while equation (13) is generally appropriate for

computing time dependence of $P_{l,k}$ it is not useful for obtaining initial conditions for the computations. Instead, we added a term

$$P_{l-1,k}/\delta t \quad (14)$$

to the term in equation (10)

$$P_{l-1,k}\left[\nu^e_{l-1,k}n_e + \nu^+_{l-1,k}n_+ + \nu^-_{l-1,k}n_-\right] \quad (15)$$

where δt refers to the time lapse since nightfall, i.e., $\delta t = i\Delta t$. The time dependence of the charge probability $P_{l,k}$ for the first few time steps (we use 10, but it is not sensitive to the number) is now approximated by the expression

$$P_{l,k} = \left[P_{l-1,k}\left(\nu^e_{l-1,k}n_e + \nu^+_{l-1,k}n_+ + \nu^-_{l-1,k}n_- + 1/\delta t\right) - P_{l-2,k}\nu^+_{l-2,k}n_+\right]/\left(\nu^e_{l,k}n_e + \nu^-_{l,k}n_-\right) \quad (16)$$

We found that this approximation is essential to initially populate the charge states. After some algebraic rearrangement, a more rigorous time differencing (semi-implicit) expression is obtained:

$$P^{j+1}_{l,k} = \Delta t\left[P^j_{l+1,k}\left(\nu^e_{l+1,k}n_e + \nu^-_{l+1,k}n_+\right) + P^j_{l-1,k}\nu^+_{l-1,k}n_+\right]/\left[1 + \Delta t\left(\nu^e_{l,k}n^j_e + \nu^-_{l,k}n^j_l + \nu^j_{l,k}\right)\right] \quad (17)$$

[17] We now have all of the equations needed to solve for n_+, n_e, and z_a. We discretize equations (1) and (2) and employ an implicit method to time step using a time step Δt of 5 s in the diffusion range and one second in the effusion range. (We define the diffusion region as the altitude region in which transport of ions and electrons is governed by collisions with atmospheric molecules. Transport of ions and electrons in the diffusion region is governed by their thermal velocities because they are likely to reach an aerosol particle before colliding with an atmospheric molecule.) With these values, all estimated errors lie within acceptable limits.

$$n^i_+ = \left(q\Delta t + n^{i-1}_+\right)/\left\{1 + \left[\alpha_{+ION}\left(n^{i-1}_+ + z_a - n^{i-1}_-\right) + \alpha_{-ION}n^{i-1}_- + d^{i-1}_{ion}\right]\Delta t\right\} \quad (18)$$

$$n^i_- = \left[\kappa n_{PAH}\left(z^{i-1}_a + n^{i-1}_+\right)\Delta t + n^{i-1}_-\right]/\left[1 + \left(\alpha_{-ION}n^{i-1}_+ + \kappa n_{PAH} + d^{i-1}_{negion}\right)\Delta t\right] \quad (19)$$

where we have used the charge neutrality condition equation (4) to eliminate n_e from equations (9) and (10). The electron density is then computed using equation (4). For the values of α_{+ION}, α_{-ION} and Δt used in our computations, the estimated error $[(\alpha_{+ION} \times n_e + \alpha_{-ION} \times n_- + d_{ion})\Delta t]^2$ is less than the order of 0.1 percent, a value that fully justifies the use of the implicit method. A discretized form of equation (5) is employed to obtain error estimates of the electron densities. This error is of the order of or less than one percent except in the altitude range in

Table 2. Estimated Mean Electron Attachment Times Versus Meridian Angle and Elapsed Time[a]

	Meridian 1	Meridian 2	Meridian 3	Meridian 4	Meridian 5
Meridian angle from dusk terminator, degrees	0.6	3.0	14.4	90 (antisolar meridian)	180 (morning terminator)
Time increment, sec	3.6×10^3	1.8×10^4	8.6×10^4	5.18×10^5	1.04×10^6
Size Bin 5					
Attachment time, sec	5×10^3	1.2×10^4	1×10^5	3.6×10^5	5.0×10^5
Size Bin 4					
Attachment time, sec	1×10^4	5×10^4	1×10^5	1×10^5	1×10^5
Size Bin 3					
Attachment time, sec	1×10^4	1.4×10^4	2×10^4	2×10^4	2×10^4

[a] Elapsed time is given in seconds elapsed from nightfall terminator, 50 km altitude. Size bin 1: No aerosol particles in bin size 1 are present at 50 km altitude. Size bin 2: Only about 10 particles m^{-3} are present at 50 km altitude.

which negative ion densities are many orders of magnitude greater than those of electrons (where the maximum error for the estimated electron density is about 15 percent). The superscripts i and i − 1 refer to the time steps. The values of α_{+ION}, α_{-ION}, and κ as well as mobilities and diffusivities are presented in Appendix B. Recombination coefficient α_{+ION} includes three-body as well as dissociative recombination.

5. Results of Time-Dependent Calculations at the Antisolar Meridian

[18] Tables 2 and 3 compare the epochs (elapsed time from the terminator) and meridian angle from the nightfall terminator with the computed characteristic electron attachment times, t_{attach} for the mean charges associated with each particle bin.

$$t_{attach} = 1.0 / \left(\sum_1 n^e_{l,k} P^i_{l,k} N^a_k \right) \qquad (20)$$

[19] Meridian angles and corresponding epochs from the terminator are provided in the top two rows of Tables 2 and 3. The estimated mean electron attachment times given by equation (20) are provided for each size bin in the subsequent rows. The attachment times increase with increasing nocturnal angles as measured from the terminator

until equilibrium is attained, provided the elapsed time is sufficiently long. Such equilibrium occurs when neutralization of negatively charged haze particles by collision with positive ions equals the attachment rate of electrons. Because of Titan's rotation the duration of night is only about 10 hours; as a result equilibrium is not attained although it is approached. The purpose of the tables is to validate our time-dependent method for computing $P_{l,k}$ and thus the electrical charging of the haze particles.

[20] Tables 2 and 3 compare the epochs and meridian angle from the dusk terminator nightfall with the computed characteristic electron attachment times, t_{attach} for the mean charges associated with each particle bin.

[21] These values show that the attachment times depend on altitude, aerosol size, and the epoch. The reason for the dependence on epoch is best illustrated by Figures 3 and 4. These figures show the time history of the charge states for bin 5 aerosols as they become fully charged. Figure 3 shows that in the diffusion dominated region, the comparatively slow charging states (i.e., those with high charge values are not in steady state). In particular the fraction with high charge values is still increasing and removing charge from the less charged states. It is clear that steady state has not yet been attained even at the subsolar meridian. (As shown by Figure 10, to be discussed in section 6, the steady state peak charge lies between −7 and −8.) On the other hand, Figure 4, which characterizes the effusion region, shows

Table 3. Estimated Mean Electron Attachment Times Versus Meridian Angle and Elapsed Time[a]

	Meridian 1	Meridian 2	Meridian 3	Meridian 4	Meridian 5
Meridian angle from dusk terminator, degrees	0.6	3	14.4	90 (antisolar meridian)	180 (morning terminator)
Time increment, sec	3.6×10^3	1.8×10^4	8.64×10^4	5.18×10^5	1.04×10^6
Size Bin 5					
Attachment time, sec	9×10^3	1.8×10^4	5×10^4	5.5×10^4	5.6×10^4
Size Bin 4					
Attachment time, sec	4.2×10^3	2.5×10^4	4.8×10^4	4.9×10^4	5×10^4
Size Bin 3					
Attachment time, sec	7×10^3	1.2×10^4	1.5×10^4	1.6×10^4	1.6×10^4
Size Bin 2					
Attachment time, sec	7×10^3	8×10^3	6×10^4	1×10^5	1×10^5
Size Bin 1					
Attachment time, sec	1×10^2	1×10^2	1×10^2	1×10^2	1×10^2

[a] Time is given in seconds elapsed from nightfall terminator, 150 km altitude.
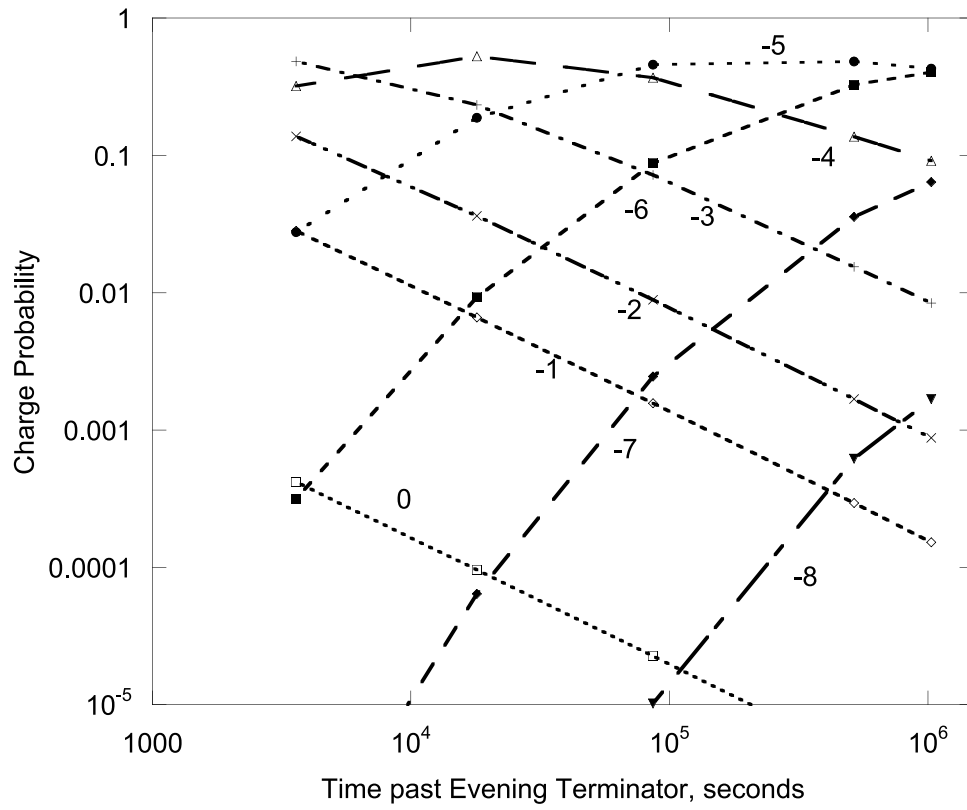
Figure 3. Time evolution of probability of charge on aerosol particles at 50 km altitude, size bin 5.
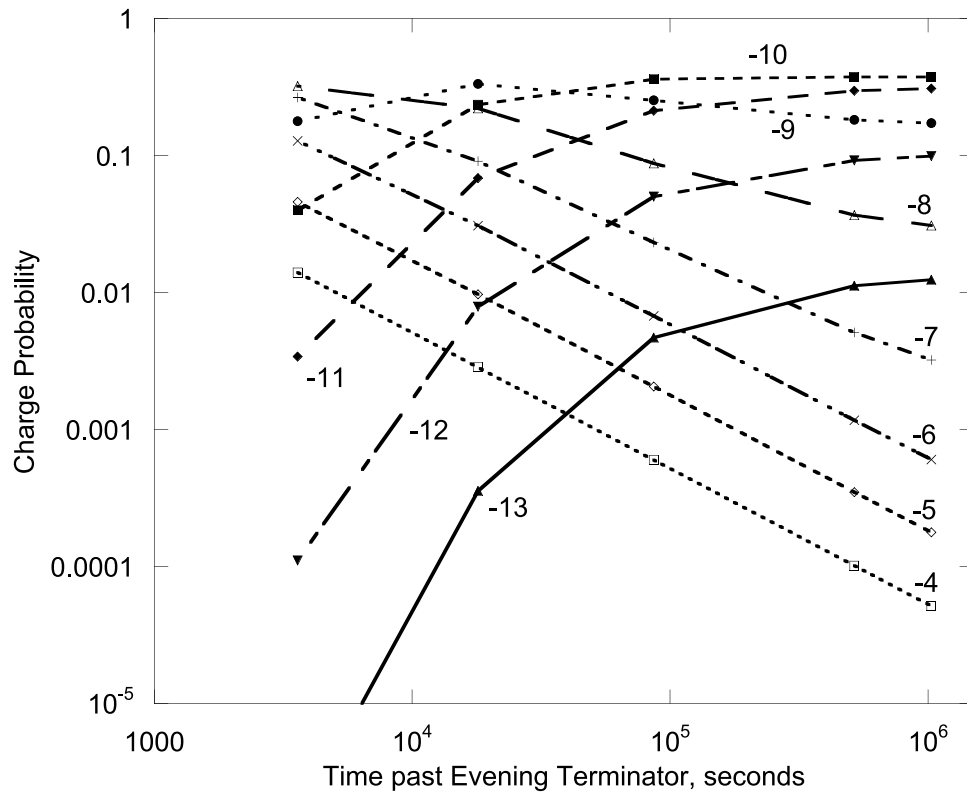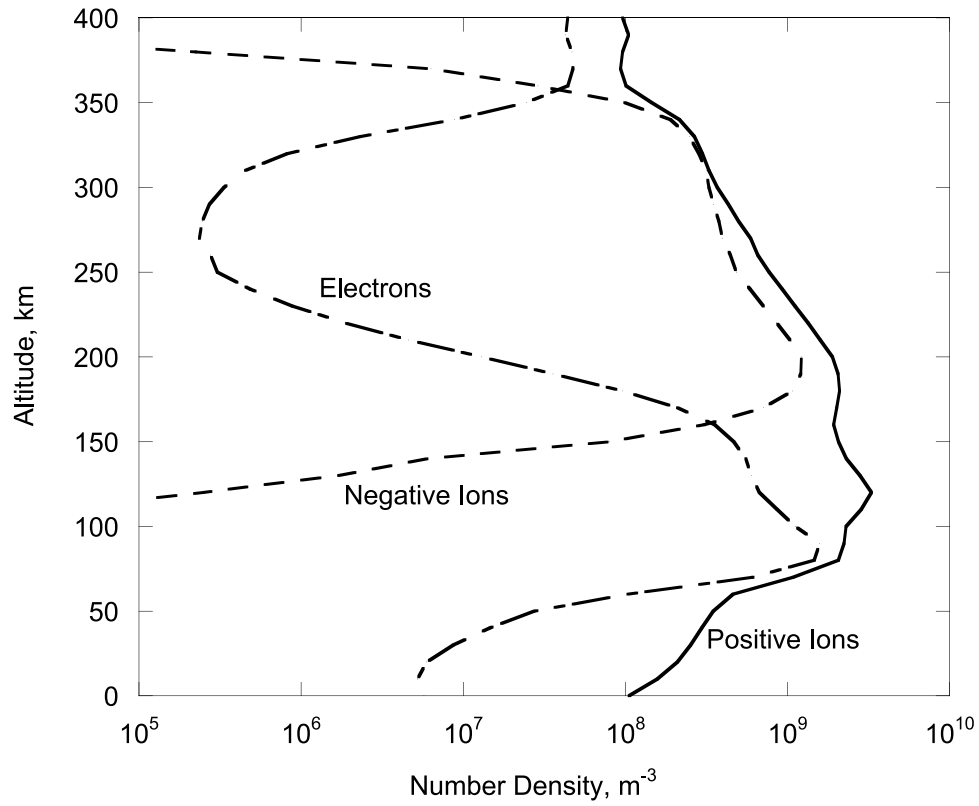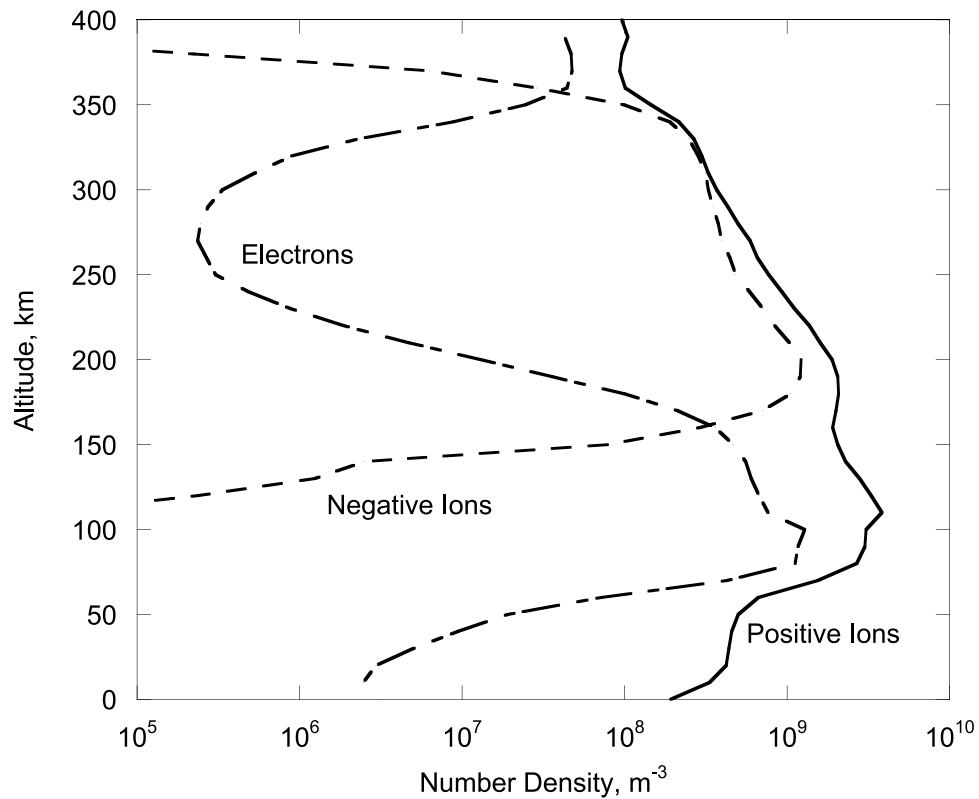

Figure 4. Time evolution of probability of charge on aerosol particles at 150 km altitude, size bin 5.

Figure 5. Computed electron, positive ion, and negative ion number densities near the antisolar meridian.

Figure 6. Electron, positive ion, and negative ion number densities at steady state.

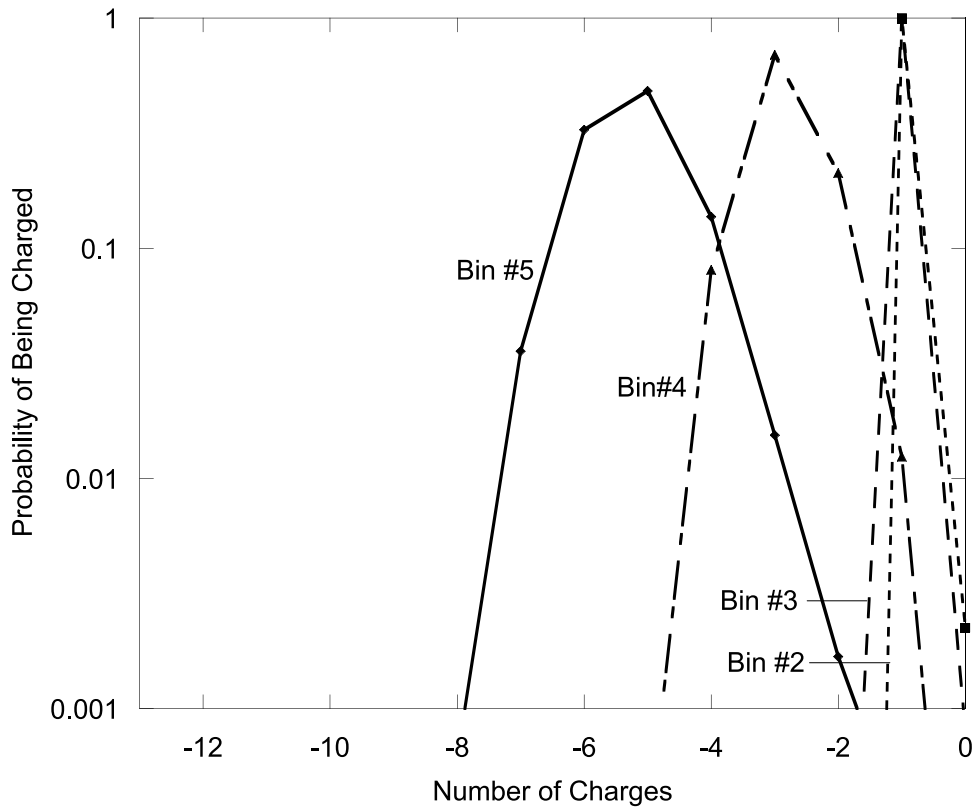**Figure 7.** Nighttime charge distributions for various particle bin sizes at 50 km altitude near the antisolar meridian.
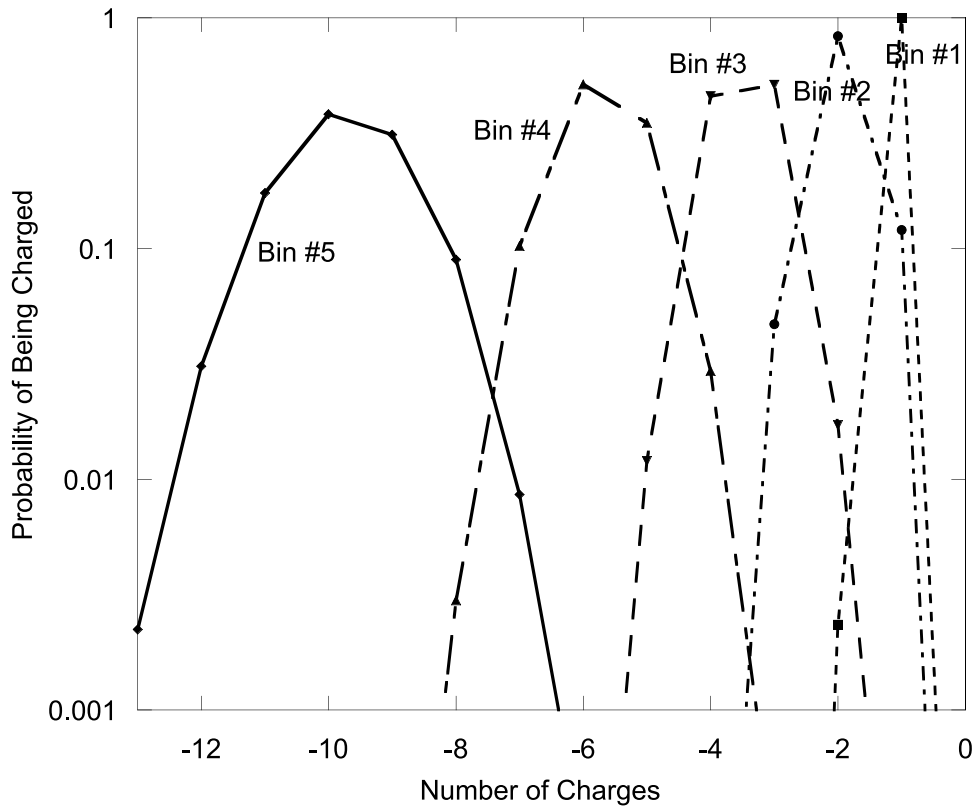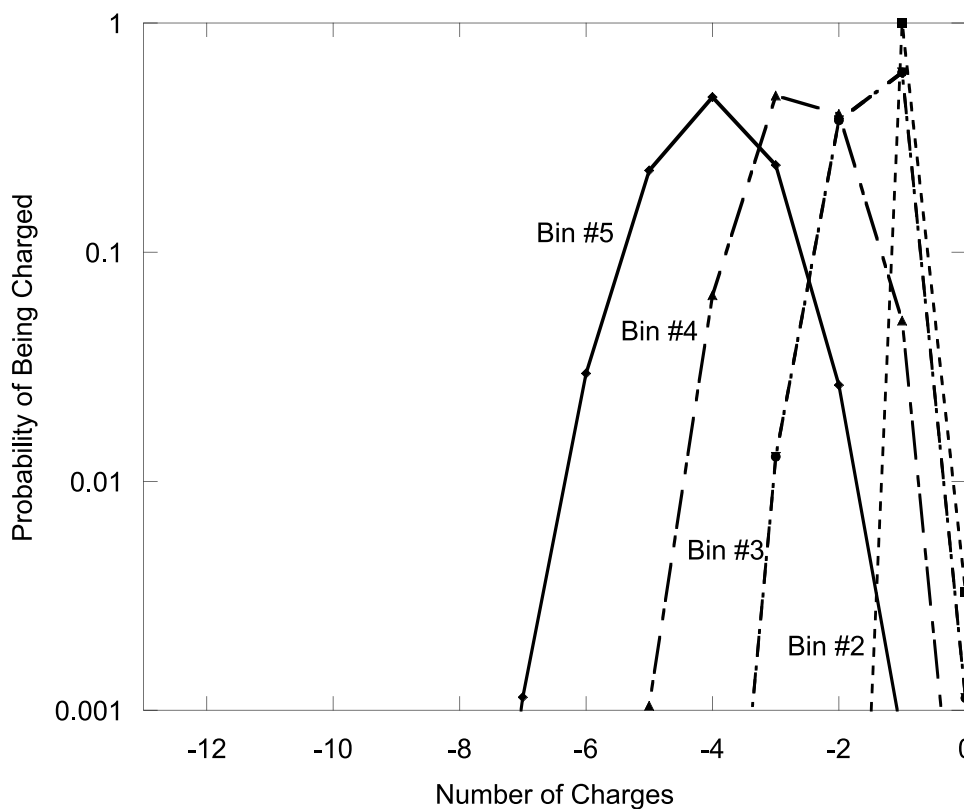

Figure 8. Nighttime charge distributions for various particle bin sizes at 150 km altitude near the antisolar meridian.

Figure 9. Nighttime charge distributions for various particle bin sizes at 250 km altitude near the antisolar meridian.

that steady state is almost attained by the time the antisolar meridian is reached.

[22] The computed values for the electron, positive ion and negative ion densities near the antisolar meridian ($\sim 5 \times 10^5$ seconds ^{s} after nightfall) are shown in Figure 5 while Figure 6 illustrates the computed densities at steady state. It is clear from these figures that the system is very close to steady state at altitudes of 150 and higher but is not quite as close at lower altitudes (the diffusion region).

[23] The outstanding feature in these density profiles is the large "bite-out" in electron density which occurs at altitudes between 170 and 350 km as a result of attachment of electrons to PAHs to form negative ions. We call these particles "negative ions" because their masses and mobilities are comparable to the masses of the positive ions. The densities of positive ions and electrons are quite similar above 350 km altitude because there are few aerosol particles at those altitudes to attach electrons. At low altitudes, the positive ion and electron densities decrease rapidly with decreasing altitude because of three-body ion-electron recombination which is proportional to atmospheric density. It should be noted that the positive ion number density in the region 160 to 220 km increases slightly with altitude. The reason for this increase is that the positive ion – negative ion recombination coefficient is an order of magnitude larger than the dissociative recombination coefficient (see Table B2 in Appendix B). Ordinarily the ion-ion recombination coefficient is smaller than the ion-electron recombination coefficient; however, the large size of the PAHs leads to a larger ion-ion recombination coefficient. Since recombination with negative ions is the dominant loss

mechanism for positive ions in the range 160 to 360 km, the loss rate is decreased and the positive ion density is larger than it would be if electrons were the dominant negative particles.

[24] Figures 7–9 show the distributions of charge on the aerosol particles at altitudes of 50, 150 and 250 km at the antisolar meridian. These altitudes were chosen for presentation because, with respect to charged particle transport properties, 50 km is in the diffusion range, 150 km is within the effusion range with very few negative ions present, while 250 km lies within the effusion range with near maximum abundance of negative ions. Although these graphs are plotted as continuous curves for clarity, only integral charge values are possible. The bin numbers refer to mean particle size as indicated in Table 1.

[25] The charge distributions for 50 km do not include bin 1 because no aerosol particles of that size are present below about 80 km. The abundance of particles in bin 2 is much less then $10^4 \, m^{-3}$ (see Figure 2). Since 50 km altitude lies within the diffusion range, diffusing electrons collide with the more abundant large particles much more frequently than the smaller particles in bin 2. Thus the larger particles accumulate the available electrons at the expense of the smaller ones. The corresponding reduced electron density at 250 km leads to reduced peak aerosol particle charges as shown in Figure 9.

[26] The formation of negative ions by attachment of electrons to very small (of the order of 3×10^{-4} microns) which we call "embryos" was investigated by *Bakes and Tielens* [1994, 1998] in the context of the interstellar medium. Later, *Bakes et al.* [2002] applied the results to
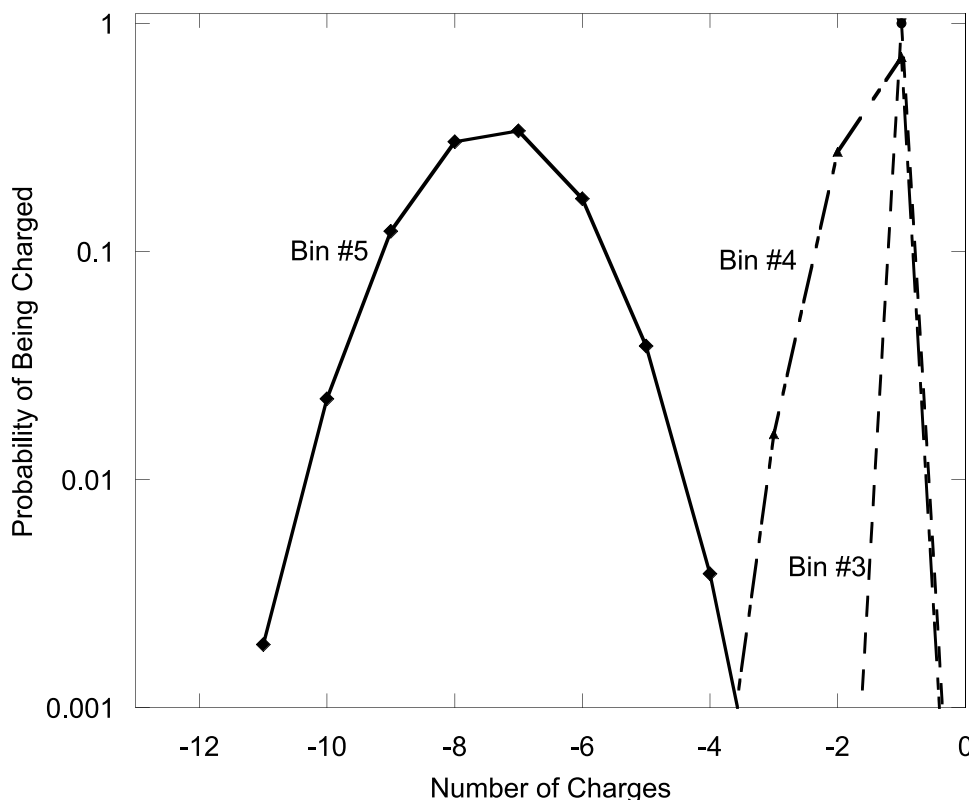
Figure 10. Nighttime charge distributions for various particle bin sizes at 50 km altitude at steady state.

the Titan haze while *Borucki et al.* [2006] employed self-consistent computations for the dayside of Titan. The latter found that negative ions are not likely to be important on the dayside if photoelectron emission is significant. The present work extends the earlier work in that we have used a time-dependent self-consistent approach discussed previously.

[27] Note that the maximum charges at 250 km altitude are substantially smaller than at 150 km despite both altitudes lying within the effusion range. The smaller maxima at 250 km occur because the electron densities are much smaller than at 150 km as a result of transfer of negative charge to the PAHs to form negative ions. The charge distributions for bin 1 (not shown because it coincides with that for bin 2) and bin 2 peak at −1 charge and are partially hidden by the distribution curves for other size bins. The mobility of the negative ions and thus the rate of attachment to aerosol particles is not large enough to produce the large negative charges aerosol particles that would occur if PAHs were not present. The somewhat similar appearance of the charge distributions at 50 km and 250 km is coincidental.

6. Comparison With Steady-State Calculations

[28] The reason for using the time-dependent approach to estimate the steady state values is that at altitudes where negative ions are abundant, estimated errors in the electron and ion densities are unacceptably large at some altitudes when the steady state method is used. As we have seen, carrying out the computations to 12 days ($\sim 10^6$ s) simulates steady state conditions very well and the excessive error problem is avoided. The increase in positive ion density

with increasing altitude in the range 160 to 220 km was explained in the discussion of Figure 6.

[29] To directly solve for the steady state conditions below 160 km, we employed the mathematical routine described in some detail in *Borucki et al.* [2006]. In brief, this routine, used to solve the coupled set of equations (1) to (4) and (9), is based on a multidimensional minimization of a function of the dependent variables, i.e., positive ion density, electron density, total charge on the aerosol particles; and the density of the negative ions (if present). The downhill simplex method of *Nelder and Mead* [1965] requires only the value of the function to be minimized and not the derivative of the function.

[30] At higher altitudes we used the computations for 2.5×10^6 seconds [s] (30 Earth days) as the steady state result. In the "overlap region (100 to 150 km) the results for the two methods were within about 5 percent of each other."

[31] The steady state electron and ion densities as well as the aerosol charges apply to both the dayside and nightside if photoemission of electrons on the dayside is absent. Such would certainly be the case if the photoemission threshold exceeds the methane cut-off ($\sim$8.7 eV). Some of our calculations indicate that a photoelectron emission threshold as small as $\sim$7 eV would render photoemission of minor importance. If the ionization potential of the aerosol particles exceeds the absorption energy cut-off for methane, ionizing solar UV radiation is absorbed in the atmosphere before it can ionize the aerosol particles and nighttime conditions apply. First results from *Fulchignoni et al.* [2005] show surprisingly small conductivities. If this result stands up, it implies that photoionization cannot be important in the Titan atmosphere.
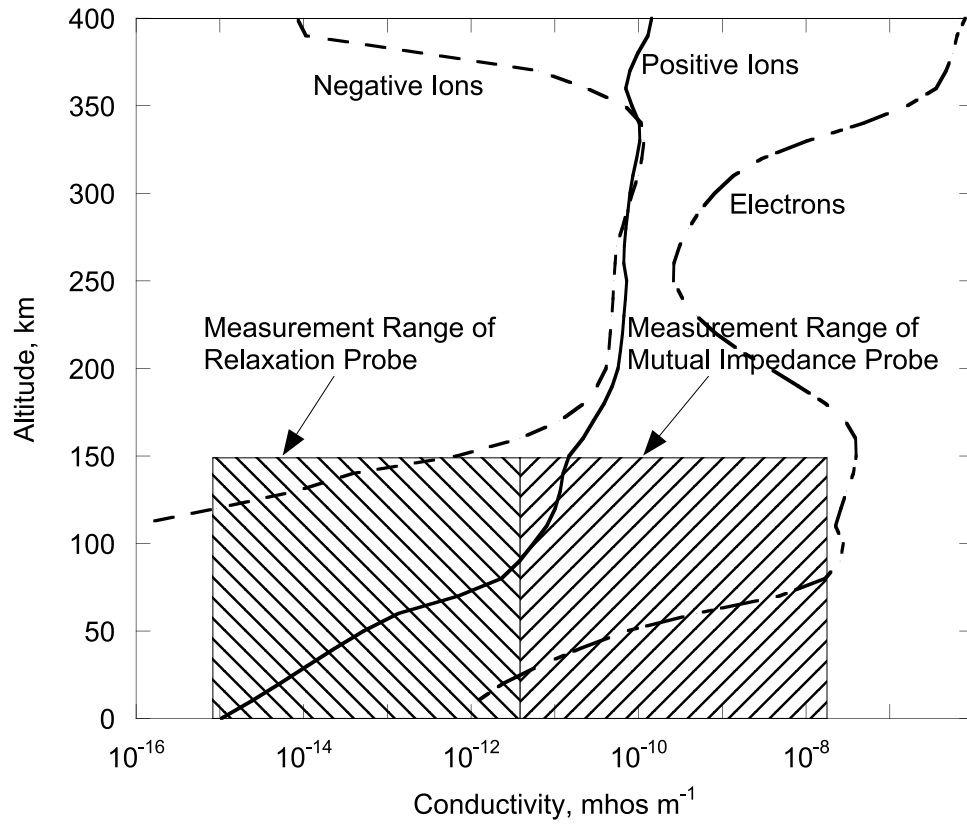
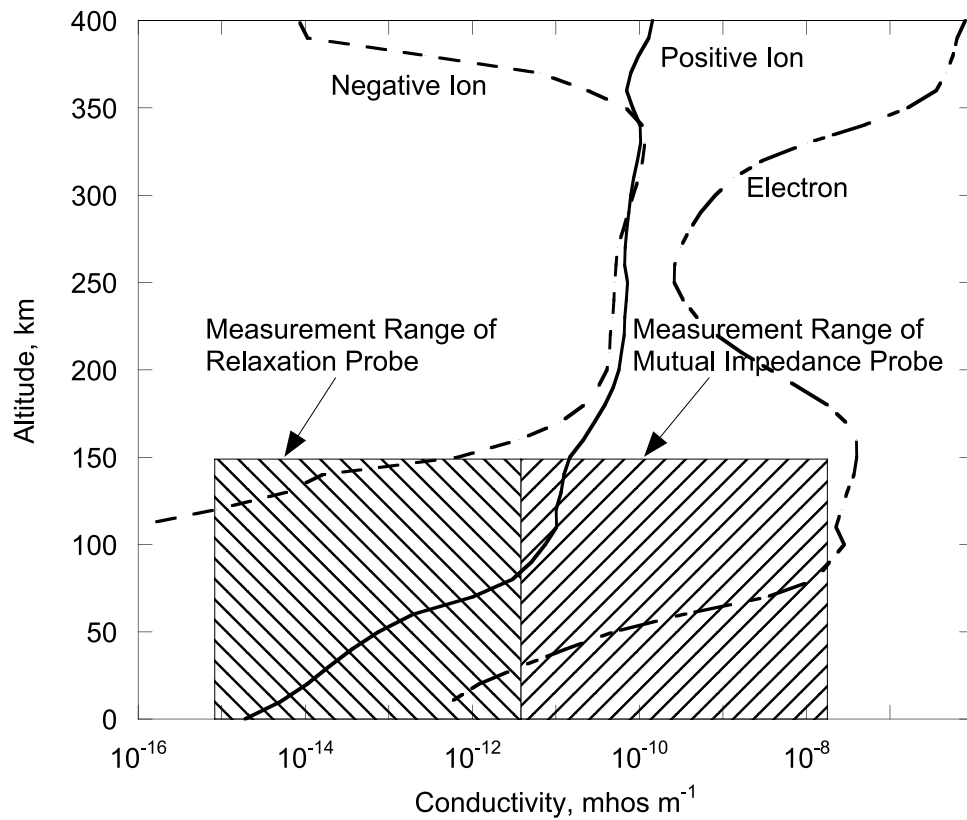**Figure 11.** Nighttime ion and electron conductivities near the antisolar meridian.

Figure 12. Nighttime ion and electron conductivities at steady state.

[32] The electron, positive ion and negative ion densities at steady state were shown in Figure 6. The ion and electron densities are quite close for the steady state and time-dependent cases, indicating that the ion and electron densities are close to equilibrium at the antisolar meridian for altitudes in the effusion region.

[33] The charge distributions on the aerosol particles at altitudes of 150 and 250 km are very close to those illustrated in Figures 8 and 9. However, at 50 km (in the diffusion range), the charge distribution on the largest particles (bin 5) broadens as shown in Figure 10. As the aerosol charge evolves, the largest particles accumulate more of the charge at the expense of charge on the smaller particles (bins 2 to 4), a result that is not surprising given the low abundance of the smaller particles at low altitudes (cf. Figure 2). The decreased electron density at low altitudes is also accounted for by the increased charge on the larger (bin 5) particles.

7. Electron and Ion Conductivities

[34] The electron and ion conductivities together with the measurement capabilities of the mutual impedance and relaxation probes on the Huygens Atmospheric Structure Instrument (HASI) are shown in Figure 11 for the antisolar meridian and Figure 12 for steady state. (HASI instrument parameters are taken from *Fulchignoni et al.* [2005].) Because the Huygens Probe entered the atmosphere on the dayside, these conductivity values would agree with those measurements only if the ionization potential of the aerosol were so high (>8.7 eV) that photoemission did not occur. The measurement of electrical conductivity by the Huygens Probe instrumentation, which would probably be employed by future atmospheric probes, is described as follows:

[35] 1. The mutual impedance instrument uses two transmitter electrodes to apply a known alternating current (45 to 5780 Hz) to the atmospheric medium. It then measures the amplitude and phase shift with two receiver electrodes. The electrical conductivity is extracted by means of Fourier transform analysis. This instrument is sensitive to high values of the conductivity; i.e., to the electron conductivity in this situation.

[36] 2. The relaxation probe sensors mounted on booms measure ion conductivity by measuring the electric charge relaxation time constant of the atmospheric medium. The charge on the electrodes is then allowed to dissipate as a result of the electric conductivity of the atmosphere, with the time constant measured by a DC electrometer amplifier. This measurement provides a measure of the positive ion conductivity as well as the combined conductivity of the negative ion and electrons.

[37] 3. First results from The HASI PWA conductivity measurements [*Fulchignoni et al.*, 2005] showed a maximum at 60 km altitude with marked decreases above and below that altitude. If these results are confirmed, they imply that photoionization is not important source of electrons in the Titan atmosphere.

8. Summary and Conclusions

[38] The results obtained for nighttime conditions are summarized as follows:

[39] 1. A time-dependent model of the charging of aerosol particles employing a modification of Parthasarathy's recurrence has been used to compute the aerosol charging on the nightside at altitudes below 150 km. The relatively long ion and electron attachment times at low altitudes requires the inclusion of time dependence for small angles measured from the evening terminator. At the antisolar meridian, electron and ion densities are very close to steady state in the effusion region but not in the diffusion region.

[40] 2. Electron densities are predicted to be much smaller on the nightside than on the dayside since GCR are the only source of ionization. They are similar if photoionization does not occur because the photoemission threshold is too large (>7 eV).

[41] 3. Aerosols are charged negatively on the nightside in contrast to the dayside where photoemission causes them to be positively charged [*Borucki et al.*, 2006].

[42] 4. Positive ion densities are somewhat greater at night than on the dayside; This effect results from the much smaller loss rate for the ions since their principal loss mechanism is recombination with electrons and the electron densities are much smaller on the nightside.

[43] 5. Given the distribution and characteristics of PAHs assumed in this paper, a very large reduction in the electron densities between 150 and 350 km is predicted.

[44] 6. Predicted conductivities appear to be within the measurement range of the relaxation and mutual impedance probes. Quantitative comparisons await publication of numerical results from the probes.

[45] 7. Although we have not included the influence on haze particle coagulation of the electrical charging of the particles, we recognize that this effect is likely to be an important mechanism for such processes. It should be included in future studies of haze particle coagulation.

Appendix A

[46] The model atmosphere used in the studies reported here is provided in Table A1. It is taken from *Yelle et al.* [1996].

Table A1. Model Atmosphere

Altitude, km	Pressure, bar	Temperature, K	Mass Density, kg m^{-3}	{N2 + CH4}, m^{-3}
0	1.46E + 00	93.28	5.44	1.16×10^{26}
20	4.84E−01	76.43	2.16	4.68×10^{25}
40	1.41E-01	70.66	0.673	1.46×10^{25}
60	4.19E-02	76.87	0.183	3.96×10^{24}
80	1.77E-02	123.61	4.79E-01	1.40×10^{24}
100	9.43E-03	142.06	2.22E-01	4.80×10^{23}
120	5.35E-03	151.00	1.18E-01	2.56×10^{23}
140	3.15E-03	158.55	6.65E-01	1.44×10^{23}
160	1.91E-03	163.77	3.90E-01	8.43×10^{22}
180	1.18E-03	167.30	2.36E-01	5.10×10^{22}
200	7.42E-04	170.48	1.46E-01	3.11×10^{22}
220	4.73E-04	172.58	9.13E-02	2.88×10^{22}
240	3.05E-04	175.42	5.82E-02	1.24×10^{22}
260	1.99E-04	177.02	3.76E-02	1.03×10^{22}
280	1.31E-04	177.97	2.46E-02	6.74×10^{21}
300	8.70E-05	178.19	1.63E-02	3.58×10^{21}
320	5.80E-05	177.63	1.09E-02	2.39×10^{21}
340	3.88E-05	176.21	7.36E-03	1.61×10^{21}
360	2.60E-05	173.85	5.00E-03	1.10×10^{21}
380	1.74E-05	170.60	3.41E-03	7.48×10^{20}
400	1.16E-05	166.61	2.33E-03	5.11×10^{20}

Table B1. Calculated Values of the Mobilities and Diffusivities of the Ion Clusters and Electrons

Altitude, km	Positive Ion Mobility, $m^2/v/s$	Electron Mobility, $m^2/v/s$	Negative Ion Mobility, $m^2/v/s^a$	Positive Ion Diffusivity, m^2/s	Electron Diffusivity, m^2/s	Negative Ion Diffusivity, m^2/s^a
0	6.180e-5	8.300e-1		4.970e-7	6.670e-3	
10	9.440e-5	1.410e + 0		6.760e-7	1.010e-2	
20	1.560e-4	2.520e + 0		1.030e-6	1.660e-2	
30	2.730e-4	4.650e + 0		1.700e-6	2.900e-2	
40	4.990e-4	8.690e + 0		3.040e-6	5.300e-2	
50	9.380e-4	1.620e + 1		5.770e-6	9.960e-2	
60	1.840e-3	2.950e + 1		1.220e-5	1.960e-1	
70	4.060e-3	4.930e + 1		3.640e-5	4.420e-1	
80	7.010e-3	7.250e + 1		7.480e-5	7.730e-1	
90	0.011	1.010e + 2		1.230e-4	1.180e + 0	
100	0.015	1.380e + 2	8.220e-3	1.850e-4	1.690e + 0	1.010e-4
110	0.017	1.850e + 2	0.019	2.110e-4	2.340e + 0	2.370e-4
120	0.019	2.450e + 2	0.018	2.500e-4	3.180e + 0	2.340e-4
130	0.026	3.190e + 2	0.028	3.490e-4	4.310e + 0	3.790e-4
140	0.034	4.150e + 2	0.034	4.660e-4	5.670e + 0	4.690e-4
150	0.045	5.350e + 2	0.047	6.260e-4	7.470e + 0	6.520e-4
160	0.070	6.860e + 2	0.066	9.930e-4	9.700e + 0	9.310e-4
170	0.090	8.750e + 2	0.081	1.290e-3	1.250e + 1	1.150e-3
180	0.116	1.110e + 3	0.107	1.680e-3	1.600e + 1	1.540e-3
190	0.148	1.410e + 3	0.134	2.160e-3	2.050e + 1	1.950e-3
200	0.188	1.770e + 3	0.171	2.760e-3	2.600e + 1	2.520e-3
210	0.238	2.230e + 3	0.216	3.530e-3	3.300e + 1	3.210e-3
220	0.300	2.780e + 3	0.273	4.480e-3	4.160e + 1	4.080e-3

[a]The abundance of negative ions is negligible below 100 km.

Table B2. Values of the Recombination and Attachment Coefficients

Coefficient	Value
α_{Dissoc}	4×10^{-12} m^3 s^{-1}
α_{3body}	$2 \times 10^{-37}(300/T)$ $[N_2]$ m^3 s^{-1}
α_{-ION}	4×10^{-13} m^3 s^{-1}
κ	6×10^{-12} m^3 s^{-1}

Appendix B

[47] The positive and negative ion mobilities (K_+ and K_-, respectively) were discussed in *Borucki et al.* [2006] and are not repeated here.

[48] Table B1 presents some calculated values for the ion and electron mobilities and diffusivities as a function of altitude. The much higher values of the electron mobility and diffusivity cause the aerosols to be charged negatively at all altitudes during the night time when no solar flux is available to photoionize the aerosols and ions.

[49] The values of α_{Dissoc}, α_{3body}, $\alpha_{-\mathrm{ION}}$, and κ are listed in Table B2. Here [N_2] is the concentration of nitrogen molecules and $\alpha_{+\mathrm{ION}} = \alpha_{\mathrm{Dissoc}} + \alpha_{\mathrm{3body}}$.

References

Bakes, E. L. O., and A. G. G. M. Tielens (1994), The photoelectric heating mechanism for very small graphitic grains and polycyclic aromatic hydrocarbons, *Astrophys. J.*, *427*, 822–838.

Bakes, E. L. O., and A. G. G. M. Tielens (1998), The effects of polycyclic aromatic hydrocarbons on the chemistry of photodissociation regions, *Astrophys. J.*, *499*, 258–266.

Bakes, E. L. O., C. P. McKay, and C. W. Bauschlicher (2002), Photoelectric charging of submicron aerosols and macromolecules in the Titan haze, *Icarus*, *157*, 464–475.

Barth, E. L., and O. B. Toon (2003), Microphysical modeling of ethane ice clouds in Titan's atmosphere, *Icarus*, *162*, 94–113.

Borucki, W. J., Z. Levin, R. C. Whitten, R. G. Keesee, L. A. Capone, A. L. Summers, O. B. Toon, and J. Dubach (1987), Predictions of the electrical conductivity and charging of the aerosols in Titan's atmosphere, *Icarus*, *72*, 604–622.

Borucki, W. J., R. C. Whitten, E. L. O. Bakes, E. Barth, and S. Tripathi (2006), Predictions of the electrical conductivity and charging of the aerosols in Titan's atmosphere, *Icarus*, *181*, 527–544.

Cabane, M., E. Chassefiere, and G. Israel (1992), Formation and growth of photochemical aerosols in Titan's atmosphere, *Icarus*, *96*, 176–189.

Cabane, M., P. Rannou, E. Chassefiere, and G. Israel (1993), Fractal aggregates in Titan's atmosphere, *Planet. Space Sci.*, *41*, 257–267.

Fulchignoni, M., et al. (2005), In situ measurements of the physical characteristics of Titan's environment, *Nature*, *438*, 785–791.

Krimingis, S. M., J. F. Carbary, E. P. Keath, T. P. Armstrong, L. J. Lanzerotti, and G. Gloeckler (1983), General characteristics of hot plasma and energetic particles in the Saturnian magnetosphere: Results for Voyager spacecraft, *J. Geophys. Res.*, *88*, 8871–8892.

Molina-Cuberos, G. J., J. J. Lopez-Moreno, R. Rodrigo, and L. M. Lara (2000), Influence of electrophilic species on the lower atmosphere of Titan, *Geophys. Res. Lett.*, *27*, 1351–1354.

Nelder, J. A., and R. Mead (1965), A simplex method for function minimization, *Comput. J.*, *7*, 308–313.

O'Brien, K. (1971), Cosmic-ray ionization in the atmosphere, *Nuovo Cimento A*, *3*, 521–547.

O'Brien, K. (1972), Propagation of muons underground and the primary cosmic-ray spectrum below 40 TeV, *Phys. Rev. D*, *5*, 597–605.

O'Brien, K. (1975a), The cosmic ray field at ground level, in *Natural Radiation Environment II*, *USERDA Rep. CONF-72085*, part 1, pp. 15–54, U.S. Dept. of Comm., Natl. Tech. Inf. Serv., Springfield, Va.

O'Brien, K. (1975b), Calculated cosmic-ray pion and proton fluxes at sea level, *J. Phys. A Math. Gen.*, *8*, 1530–1534.

Parthasarathy, R. (1976), Mesopause dust as a sink for ionization, *J. Geophys. Res.*, *81*, 2392–2396.

Rages, K., and J. B. Pollack (1983), Vertical distribution of scattering hazes in Titan's upper atmosphere, *Icarus*, *55*, 50–62.

Rages, K., J. B. Pollack, and P. H. Smith (1983), Size estimates of Titan's aerosols based on Voyager high-phase angle images, *J. Geophys. Res.*, *88*, 8721–8728.

Tomasko, M. G., and P. H. Smith (1982), Photometry and polarimetry of Titan: Pioneer 11 observations and their implication for aerosol properties, *Icarus*, *51*, 65–95.

Toon, O. B., C. P. McKay, C. A. Griffith, and R. P. Turco (1992), A physical model of Titan's aerosols, *Icarus*, *95*, 24–53.

Vogt, R. E., D. L. Chenette, A. C. Cummings, T. L. Garrard, E. C. Stone, A. W. Schardt, J. H. Trainor, N. Lal, and F. B. McDonald (1981), Energetic charged particles in Saturn's magnetosphere: Voyager 1 results, *Science*, *212*, 231–234.

West, R. A., A. L. Lane, H. Hart, K. E. Simmons, C. W. Hord, D. L. Coffeen, L. W. Esposito, M. Sato, and R. B. Pomphrey (1983), Voyager 2 photopolarimeter observations of Titan, *J. Geophys. Res.*, *88*, 8699–8708.

Yelle, R. V., D. F. Strobell, E. Lellouch, and D. Gautier (1996), Engineering models for Titan's atmosphere, *Eur. Space Agency Spec. Publ.*, *ESA SP-1177*, 243–256.

———————————

W. J. Borucki, NASA Ames Research Center, M.S. 244-30, Moffett Field, CA 94035, USA.

S. Tripathi, Indian Institute of Technology, Kanpur -208016, India.

R. C. Whitten, SETI Institute, 515 N. Whisman Road, Mountain View, CA 94043, USA. (rwhitten@pacbell.net)